International Journal of Biomedical Engineering and Technology

ISSN online: 1752-6426 - ISSN print: 1752-6418
https://www.inderscience.com/ijbet

An advanced wavelet decomposition based denoising technique for de-speckling of all ultrasound images

Mayank Kumar Singh, Indu Saini, Neetu Sood

DOI: 10.1504/IJBET.2023.10054699

Article History:

Received:	11 October 2022
Last revised:	02 January 2023
Accepted:	01 February 2023
Published online:	31 January 2024

An advanced wavelet decomposition based denoising technique for de-speckling of all ultrasound images

Mayank Kumar Singh*, Indu Saini and Neetu Sood

Department of Electronics and Communication Engineering,
Dr. B.R. Ambedkar National Institute of Technology,
Jalandhar Punjab, India
Email: mayankks.ec.19@nitj.ac.in
Email: sainii@nitj.ac.in
Email: soodn@nitj.ac.in
*Corresponding author

Abstract: The ultrasound (US) image is well known for accessibility and low cost. Most importantly it is the only diagnostic technique which is radiation free. But, the presence of speckle noise, thoroughly limits its application for diagnosis. This paper aims to remove the noise using wavelet transformation. The US were transformed using discrete wavelet transform after log transformation. A threshold was obtained using the estimated noise variance for each sub-band. A multi-scale thresholding function was proposed to increase the thresholding flexibility. A large range of US were used (12,400, 926, 780, and 1,000 images of foetus, liver, breast and synthetic images respectively) to evaluate the performance. When compared with other thresholding techniques the proposed method has shown a maximum improvement of 172%, 340%, and 380% in peak signal to noise ratio, mean square error, and structural similarity index. With the referenceless metrics our technique has shown 47% improvement in US quality.

Keywords: denoising; speckle noise; ultrasound images; wavelet transformation.

Reference to this paper should be made as follows: Singh, M.K., Saini, I. and Sood, N. (2024) 'An advanced wavelet decomposition based denoising technique for de-speckling of all ultrasound images', *Int. J. Biomedical Engineering and Technology*, Vol. 44, No. 1, pp.47–63.

Biographical notes: Mayank Kumar Singh is currently pursuing his PhD in Electronics and Communication at Dr. B.R. Ambedkar National Institute of Technology Jalandhar. He received the master of technology from Dr B.R. Ambedkar N.I.T. Jalandhar. He received the award of Bachelor of Technology from G.K.V. Haridwar in Electronics and Communication. His area of expertise are biomedical signal acquisition and processing, medical image processing, machine learning, artificial intelligence, human computer interface and evolutionary algorithm.

Indu Saini is an Assistant Professor at Department of Electronics and Communication in Dr. B.R. Ambedkar National Institute of Technology Jalandhar. She received the award of doctorate and master of technology from Dr. B.R. Ambedkar N.I.T. Jalandhar. She received the award of bachelor of technology from G.N.D.U. Amritsar in Electronics and Communication. Her areas of expertise are biomedical signal acquisition and processing, medical image processing, machine learning, artificial intelligence and evolutionary algorithm.

Neetu Sood is an Assistant Professor at Department of Electronics and Communication in Dr. B.R. Ambedkar National Institute of Technology Jalandhar. She received the award of Doctorate from Dr. B.R. Ambedkar N.I.T. Jalandhar and Master's in Engineering from Thapar Institute of Engineering and Technology, Patiala. She received the award of Bachelor of Technology from Sant Longowal Institute of Engineering and Technology in Electronics and Communication. Amritsar. Her area of expertise are biomedical signal acquisition and processing, medical image processing, machine learning, artificial intelligence, advance communication and evolutionary algorithm.

1 Introduction

Before treatment of any In Vivo disease, it is compulsory to analyse its state. It is done either by following an invasive or a non-invasive procedure (Arumugham et al., 2019; Bini, 2021). It is most reasonable to adopt a non-invasive procedure since it is painless. The non-invasive procedure for diagnosis starts with developing an image of the affected area. Later, an experienced radiologist evaluates the condition. The imaging technique here involves waves of different frequencies, which can successfully invade the skin. The most practiced imaging techniques are magnetic resonance images, computed tomography, X-rays, mammograms, and ultrasound (US) (Bini and Bhat, 2014; Perumal and Thiruvenkadam, 2022; Talbar et al., 2022; Yadav and Ganvir, 2022). The US-based imaging has many advantages over others like it is the most economical, least complex setup, hand-held transducers, and completely harmless. The only disadvantage of a US image is its quality due to the speckle noise (Yu et al., 2012).

US images suffers from two types of noises one is the additive noise and the other is multiplicative noise. Their names represent their mathematical relation with the image pixels as given in equation (1).

$$Im_o = (Im_i \times P_m) + P_a \tag{1}$$

Here, Im_o is the observed US image, Im_i is the ideal US image (uncorrupted image), P_m is the multiplicative noise and P_a is the additive noise. The zero-mean property of the additive noise makes it removal easy. Basic averaging filters can efficiently suppress the distortion due to the additive noise. In the averaging filter the pixel intensity is replaced by the average intensity of its surrounding pixel and the additive noise due to its zero average property is suppressed sufficiently. The multiplicative component also known as the speckles, are because of the internal reflection of US waves during imaging process. These unwanted reflections are received at the transducer and interpreted as granular distortion in the US image. Due to its multiplicative nature its removal is very challenging (Priestly Shan et al., 2021).

The denoising needs to be done efficiently but without losing the fine details (Chen and He, 2021). In the image, many methodologies have been proposed to date for denoising mean filters, median filters, bilateral filters (Luo et al., 2019), anisotropic diffusion (AD) (Chen and He, 2021), and wavelet thresholding (or shrinkage) (Nabil, 2013). The mean and median filters narrow down many intensity variations in the image. The bilateral filter is a nonlinear smoothing filter that has a blurring effect at the image edges. The choice of edge-stopping function is a little tricky in anisotropic diffusion, so

denoising is ineffective. Wavelet based thresholding technique on the other hand adopts multiresolution processing of the image (Nair and Singh, 2022). Images are first divided into one approximation and three detail sub-bands using wavelets. The approximation sub-band has the most of the important details of the image and negligible presence of noise, while the opposite is true for the detail sub-band. In this way the technique is significantly able to preserve the image details and successfully remove the noise at the same time.

In the wavelet thresholding framework, the thresholding function that has been used to date has limited flexibility. That is, mostly all of the studies to the best of our knowledge divide the coefficients into two scales (Andria et al., 2013; Bedi and Sunkaria, 2022; Elyasi et al., 2016; Randhawa et al., 2019; Vidakovic, 1998). But having the coefficients divided into higher scales will result in improved recovery. Moreover, the threshold value needs to be improved to divide the coefficients into higher scales. In this literature, we have introduced an advanced wavelet decomposition-based speckle reduction technique to remove noises in ultrasound images. The speckle noises are present in the ultrasound image in the form of multiplicative noise. They are first converted into additive noise. Then we introduced a hybrid threshold value for the identification of noisy coefficients. And a novel multi-scale functions to restore the noise coefficients of the sub-band. To the best of our knowledge, not a single wavelet denoising technique has been tested on this variety of US images. Moreover, we designed a large set of synthetic images with the resemblance of a breast US image to test the reference-based performance measures. The results of the proposed technique were compared with various best-in-class speckle reduction techniques.

2 Research background

Wavelet provides a multi-resolution analysis of an image (Venkatesan and Ragupathy, 2022). Hence wavelet transformation also enables the multi-resolution analysis of the effect of speckle noise. Many studies have observed a strong correlation between the variances of the detail sub-band histogram and that of speckle noise variance. So, wavelet-based methods provide a more fundamental way of reducing the effects of speckle noise. In the most cardinal procedure of the wavelet-based technique the image is transformed twice. First transformed with the logarithmic transform and then with the wavelet transformation (Jing-Yi et al., 2016). After the logarithmic transform, the nature of speckle noise changes to additive from multiplicative. It eases the further processing of the image for denoising. In the next step, a median absolute deviation based estimator (MadE) is used to estimate the speckle noise variance (Wilcox, 2022) (var_n). To date, different methods have been introduced to calculate a suitable threshold (th) from the estimated variance. Initially a VisuShrink was introduced by D.L. Donoho and I.M. Johnstone. It is also known as the universal threshold, and its calculation is in equation (2).

$$th_{univ} = var_n \sqrt{2\log(M \times N)} \tag{2}$$

The size of the input image is ($M \times N$). Later it was improved by using Stein's unbiased risk estimator (SE) (Chang et al., 2000). In the improved version, the threshold value was chosen as the minimum of th_{univ} and the value that minimises SE. It was named as

SureShrink because of the SE. D.L. Donoho and I.M. Johnstone also introduced BayesShrink (Donoho, 1995), which has its threshold value as given in equation (3).

$$th_{Bayes} = {var_n^2}\Big/{var_l} \tag{3}$$

After thresholding, a thresholding function is required to improve the noisy coefficient. Primarily there are two functions, soft and hard thresholding, in equations (4) and (5), respectively.

$$f(c) = \begin{cases} 0 & if\ |c| < th \\ c & if\ |c| \geq th \end{cases} \tag{4}$$

$$f(c) = \begin{cases} 0 & if\ |c| < th \\ sign(c)(|\,c\,| - th) & if\ |c| \geq th \end{cases} \tag{5}$$

The hard threshold produces larger discontinuities in the histogram. The soft thresholding is better than the hard thresholding in terms of discontinuities, but it also creates spikes in the histogram. These discontinuities and spikes result in poor recovery from speckle noise. Andria et al. (2013) used an exponential operator for coefficient transformation. As given in equation (6), the function was way more flexible than soft and hard thresholding in coefficient transform.

$$f(c) = \begin{cases} c.e^{k(|c| - th)} & if\ |c| < th \\ c & if\ |c| \geq th \end{cases} \tag{6}$$

Here the k is the exponential function degree of fall, the threshold is $\alpha \times th_{univ}$, and α is the flexibility parameter. α controls the threshold value and makes it more flexible than soft and hard thresholds. The Bayesian threshold has better performance than the universal threshold. So, Elyasi et al. (2016) proposed a modified threshold function and a novel framework to calculate the value. For coefficient thresholding, they adopted soft thresholding. And the soft thresholding is known for its unwanted spikes in the histogram. Randhawa et al. (2019) presented a unique threshold calculation method and a more advanced version of the exponential thresholding function. The thresholds were calculated separately for each sub-band. Instead of having a single threshold, they preferred to have a unique threshold for each sub-band. The threshold value calculation and the thresholding function are in equations (7) and (8).

$$th(S_l) = {thu_{niv}(S_l)}\Big/{\log(1+l)} \tag{7}$$

$$f(c) = \begin{cases} c.\beta^{l(|c| - th)} & if\ |c| < th \\ c & if\ |c| \geq th \end{cases} \tag{8}$$

Here, S is the sub-band and l is the level of decomposition of the image. The universal threshold is calculated for each sub-band at each level. The value β was taken within the range [1, 100], and the best outcomes were for $\beta = 7$. There has also been an attempt to apply the combination of anisotropic diffusion and wavelet thresholding to reduce speckle noise (Singh et al., 2021). The study was in 2021, where the anisotropic diffusion

was applied to the approximation sub-band. And for the rest of the sub-bands, the soft thresholding with the universal threshold was applied. The idea was unique, but the improvement observed was not very overwhelming. Another study by Bedi and Sunkaria (2022) used the exponential thresholding function as in Andria et al. (2013). Instead of calculating the threshold for each sub-band, they used a global threshold for each sub-band on the same level. The calculation of the threshold (th_{bedi}) is in equation (9).

$$th_{bedi} = 2\delta\left[\left(\left|var_n^2 - var_d^2\right|\right) \Big/ var_n\right] \tag{9}$$

Here the $\delta = \sqrt{2\log(M \times N)}$ where $M \times N$ represents the total number of pixels in the image or the length of the image.

3 Materials and method

3.1 Dataset

In this literature, we have applied the proposed technique for denoising different types of US images. We have used breast, liver, and foetus US images for performance testing. All the datasets used here are public datasets and are available online. The dataset for breast US images was made online by Al-Dhabyani et al. (2020). The dataset has a total of 780 images of the breast of different women. It contained both cancerous and non-cancerous breast US images. For the US images of the foetus, we have used the dataset provided by Burgos-Artizzu et al. (2020). The dataset comprises 12,400 images from 1,792 different patients. The dataset of liver US images is provided by Ultrasound Data of a Variety of Liver Masses (B-Mode-and-CEUS-Liver) –TCIA Public Access – Cancer Imaging Archive Wiki (n.d.). It contained 926 US images from 120 patients, and the images are in DICOM format. The datasets were made available after taking concern for patients. The mages were labelled after being critically reviewed by an expert radiologist. Apart from clinical US images, a large image set (1,000) of the synthetic image, which looks similar to breast US image was generated. Some standard images were also involved in this study.

3.2 Method

The input image I_{in} is first transformed using logarithmic transform. The logarithm transformed image I^* has the speckle noise as an additive component. This is done to reduce the computation complexity, and the operation applied to the multiplicative component will affect the image too. The log-transformed image is next divided into the sub-band using wavelet thresholding. An example of the output image after the sub-band division is given in Figure 1.

The wavelet transforms divide the image into four sub-bands, one approximation, and three detail sub-band. In Figure 1, it can be observed that the approximation (a) sub-band has most of the image details at a different resolution. And further division into sub-band is obtained after applying wavelet decomposition on the approximation band. In wavelet thresholding, this sub-band is left unchanged. Figure 2 presents the process flow of the complete proposed method. The diagonal sub-band coefficients were used for the

calculation of noise variance. Instead of using a single noise variance value for all resolutions, we have used different noise variances at each resolution. The diagonal sub-band of the corresponding resolution is used for calculating noise variance at each resolution. Hence the threshold value will be different for each resolution. The threshold value in our study comprises both the universal and the Bayesian threshold given in equation (10). If the noise variance is larger than the variance of the sub-band coefficients then the universal threshold is the threshold value. Otherwise, the Bayesian threshold is used as the threshold value. The steps to calculate the Bayesian threshold are in Elyasi et al. (2016), and the calculation of the universal threshold is in equation (1).

$$th = \begin{cases} th_{univ} & if\ var_n > var_l \\ th_{Bayes} & otherwise \end{cases} \tag{10}$$

Figure 1 The Haar wavelet transform of (a) a liver US image to decompose the image into, (b) sub bands (see online version for colours)

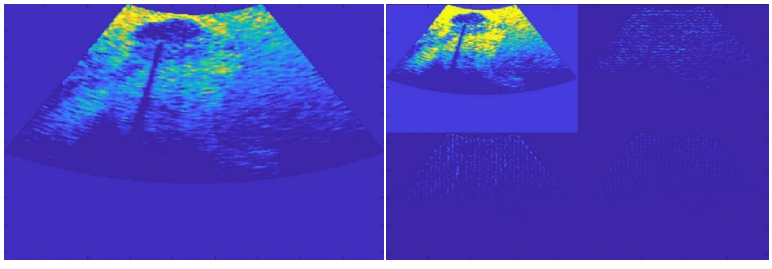

(a) (b)

Figure 2 Process flow diagram of proposed technique (see online version for colours)

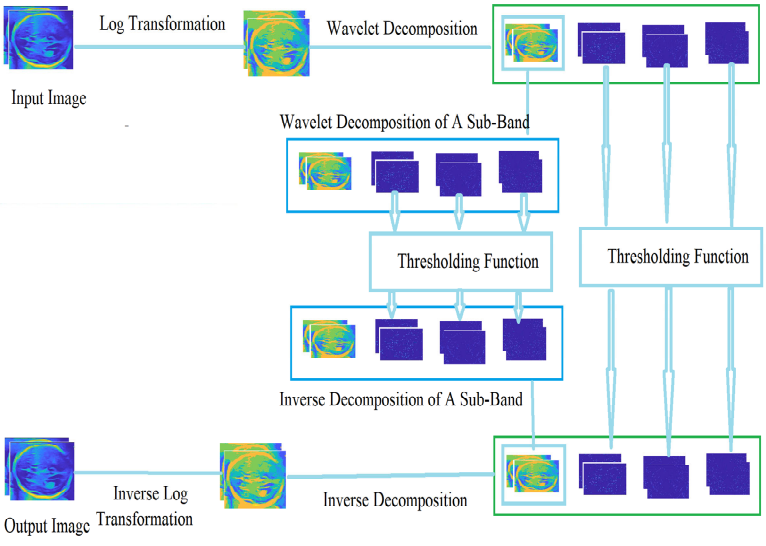

The thresholding function for the coefficient modification is a tri-scale function. For coefficients that are smaller than even half the threshold, it is replaced by 0. The

coefficients with a value larger than half of the threshold are divided into two groups, and their corresponding thresholding function is defined in equation (11). Where $\beta_{1,2}$ $a_{1,2}$ and $b_{1,2}$ are constant whose values were empirically selected.

$$w = \begin{cases} 0 & if\ w < th/2 \\ w \times \beta_1^{a_1(|w - b_1 * th|)} & if\ \dfrac{th}{2} < w < th \\ w \times \beta_2^{a_2(|w - b_2 * th|)} & otherwise \end{cases} \tag{11}$$

4 Results and discussion

Since all the US images are already affected by speckle noise, they cannot be used for full reference quality evaluation. The performance evaluation using full reference quality metrics is a must to have a noise-free reference image. And a noise-free US image in the dataset is not available, so we have used both the standard and synthetic images. To validate the performance of the proposed technique for the US images, we have used quality metrics that do not require reference images. MATLAB was used to implement the proposed algorithm, and the values of all the constants are in Table 1.

Table 1 The constants and their values

Constants	*Value*
β_1	4
a_1	2.5
b_1	4
β_2	7
a_2	3
b_2	3.2
Wavelet function	Dmeyer (Khatkar and Kumar, 2015)

For comparison, we have used the Wiener filter (Baselice et al., 2018), AD, I. Elyasi. modified shrink, G. Andria exponential shrink, S.K. Randhawa modified exponential shrink, sub-band anisotropic diffusion (SBAD), 2d version of the Gabor filter (Chen et al., 2021), and residual learning based denoising (DCNN) (Kokil and Sudharson, 2020). Table 2 has the value peak signal to noise ratio (S/N), mean squared error (M2E), and the structural similarity index (SSI) for the standard grayscale test images. Detailed information about these metrics is in Anwar and Rajamohan (2020). The proposed technique outruns all these techniques at each level of noise. Graph in Figure 3 has a better visualisation of the parameter variation with increasing noise variance. The recurrent learning-based DCNN has a little bit better performance at lower noise variance. But with increasing noise variance the proposed methodology outruns the DCNN. For the Lena image corrupted with speckle noise of variance 0.3 the proposed technique has 37% better SSI. For similar noise in Barbara image the proposed technique has 20% improved S/N than DCNN. For the highest variance of noise, the proposed methodology has S/N, MSE, and SSI of 21.5, 539.17, and 0.57 for the LENA and 30.92, 56.15, and 0.61 for the Barbara image, respectively. The performance variation of

proposed technique can be observed from the graph in Figure 3. Unlike other techniques the performance of the proposed technique does not decay rapidly. With the Lena image corrupted with a highest-level noise the proposed methodology has shown 30.7%–172%, 60%–340%, and 92%–380% improvements in S/N, M2E, and SSI, respectively with other thresholding techniques.

Table 2 Result of denoising for standard greyscale test images

Images	*Technique*	*var_n = 0.1*			*var_n = 0.2*			*var_n = 0.3*		
		S/N	*M2E*	*SSI*	*S/N*	*M2E*	*SSI*	*S/N*	*M2E*	*SSI*
Lena	G. Andria (2013)	24.8	561	0.38	20.6	712	0.29	13.7	1,102	0.16
	I. Elyasi (2016)	24.6	593	0.40	20.8	708	0.30	13.9	1,056	0.17
	S.K. Randhawa (2019)	26.4	502	0.43	22.5	581	0.34	15.8	958	0.21
	Wiener filter (2018)	25.0	517	0.41	21.9	597	0.33	16.1	928	0.21
	SBAD (2021)	19.6	795	0.30	15.7	1,468	0.27	9.2	2,327	0.10
	A.K. Bedi (2022)	29.3	276	0.69	26.4	443	0.53	19.2	847	0.25
	Gabor (2021)	25.4	497	0.46	22.3	603	0.36	15.6	1,017	0.20
	DCNN (2020)	30.8	251	0.71	27.2	363	0.57	21.2	628	0.35
	Proposed	*31.2*	*212*	*0.75*	*29*	*329*	*0.67*	*25.1*	*529*	*0.48*
Barbara	G Andria (2013)	30.3	112	0.51	25.8	256	0.43	20.1	568	0.33
	I. Elyasi (2016)	30.1	119	0.53	25.1	262	0.46	20.2	545	0.37
	S.K. Randhawa (2019)	30.8	106	0.51	26.9	238	0.44	21.6	468	0.36
	Wiener filter (2018)	31.2	91	0.5	27.4	212	0.43	23.5	432	0.33
	SBAD (2021)	29.2	232	0.47	25.7	488	0.38	19.6	786	0.26
	A.K. Bedi (2022)	31.2	85	0.73	28.3	168	0.64	25	257	0.51
	Gabor (2021))	29.8	212	0.51	27.7	413	0.43	23.6	412	0.31
	DCNN (2020)	38.2	39	0.77	32.3	121	0.67	29	198	0.55
	Proposed	*37.8*	*41*	*0.76*	*36.2*	*73*	*0.69*	*34.9*	*138*	*0.61*

We have also used a set of 1,000 (random samples of which are in Figure 4) synthetic ultrasound images developed in MATLAB using basic shapes of circles, ellipses, and sinusoidal equations. The circle and ellipse were used to create a lesion alike structure and sinusoidal waves were for muscle fibres and bones. We first developed these synthetic images and the added noises of different variances to test the algorithm's efficiency. Since we have the noise-free reference image, we calculated S/N, M2E, and SSI. Table 3 has the average S/N, M2E, and SSI values for the 1,000 synthetic images de-speckled using various algorithms. The proposed technique has 19.26% better S/N, 36.67% better M2E, and 27.27% better SSI, than the CNN-based DCNN at a noise variance of 0.3. The bar graph in Figure 5 shows the comparison of the de-speckling techniques in terms of S/N, M2E, and SSI. The S/N and M2E was normalised to construct the chart. The proposed technique outclasses other techniques with a significant margin. Figure 4 presents some of the synthetic images and their corresponding noisy and processed image.

Figure 3 (a) A line chart representing the values of (i) SSI, (ii) M2E, (iii) S/N for different techniques (wiener filter, I. Elyasi et al., G. Andria et al., S.K. Randhawa et al., A.K. Bedi et al., SBAD, Gabor, DCNN, and the proposed) for the Barbara image corrupted with various noise variance (b) A line chart representing the values of (i) SSI, (ii) M2E, (iii) S/N for different techniques (wiener filter, I. Elyasi et al., G. Andria et al., S.K. Randhawa et al., A.K. Bedi et al., SBAD, Gabor, DCNN, and the proposed) for the Lena image corrupted with various noise variance (see online version for colours)

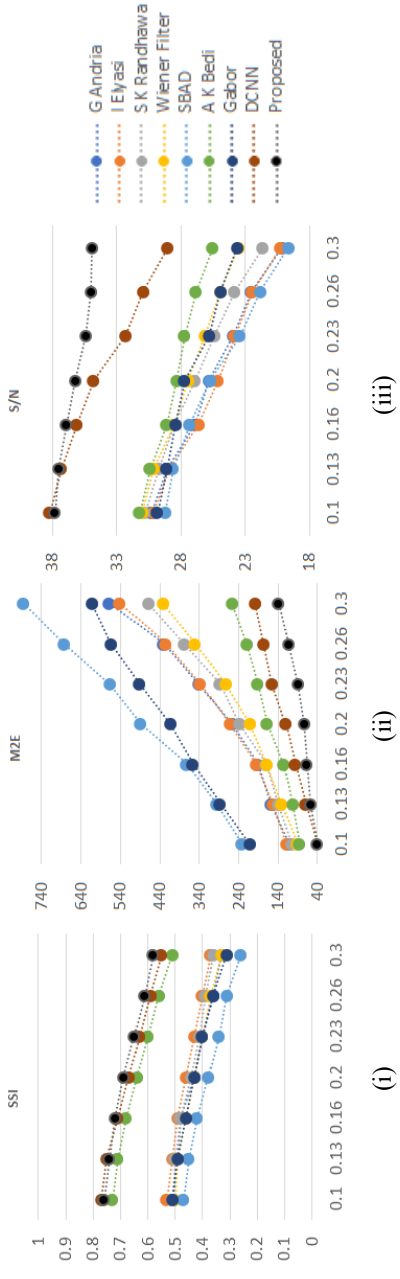

Figure 3 (a) A line chart representing the values of (i) SSI, (ii) M2E, (iii) S/N for different techniques (wiener filter, I. Elyasi et al., G. Andria et al., S.K. Randhawa et al., A.K. Bedi et al., SBAD, Gabor, DCNN, and the proposed) for the Barbara image corrupted with various noise variance (b) A line chart representing the values of (i) SSI, (ii) M2E, (iii) S/N for different techniques (wiener filter, I. Elyasi et al., G. Andria et al., S.K. Randhawa et al., A.K. Bedi et al., SBAD, Gabor, DCNN, and the proposed) for the Lena image corrupted with various noise variance (continued) (see online version for colours)

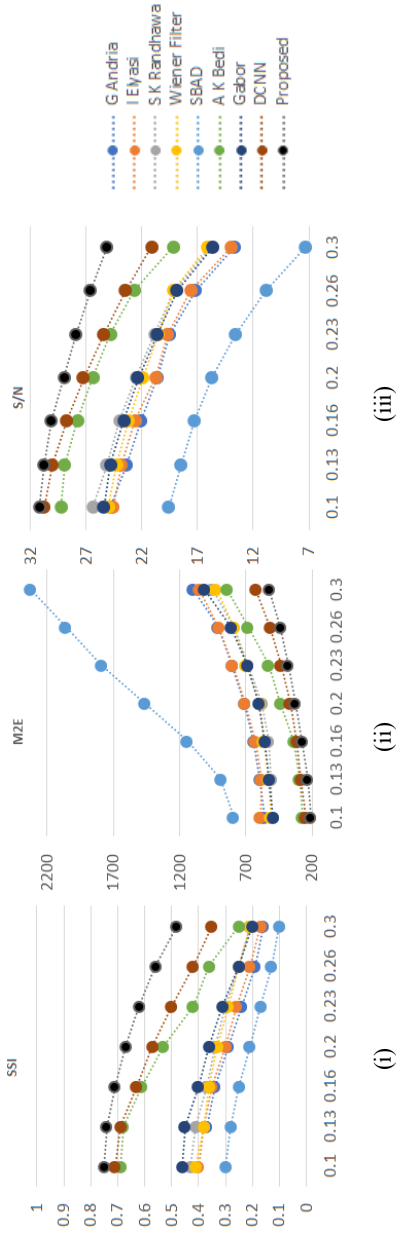

Figure 4 Output of techniques where, (a) is the original synthetic images, (b) the intentionally added speckle noise, (c) Wiener filter, (d) I. Elyasi et al., (e) G. Andria et al., (f) S.K. Randhawa et al., (g) A.K. Bedi et al., (h) SBAD, (i) Gabor, (j) DCNN, (k) proposed

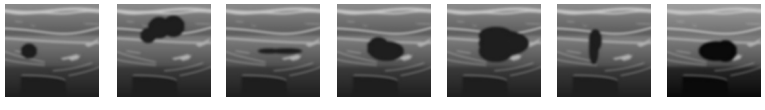

(a)

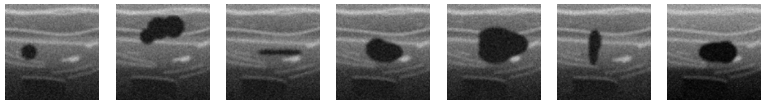

(b)

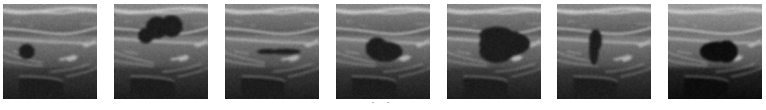

(c)

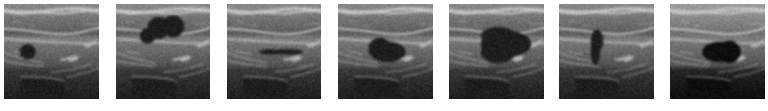

(d)

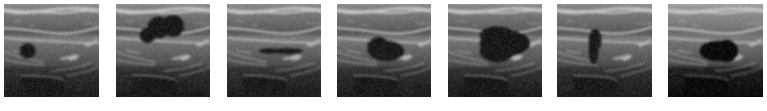

(e)

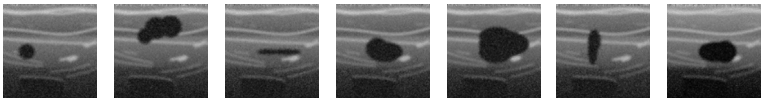

(f)

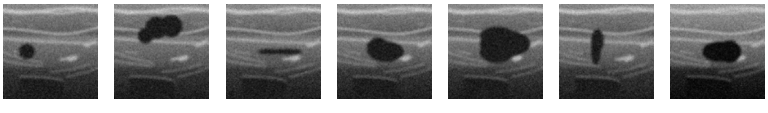

(g)

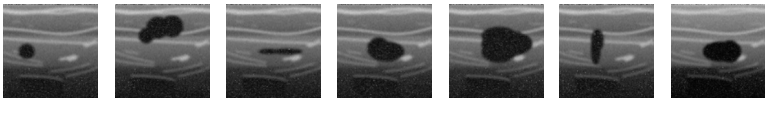

(h)

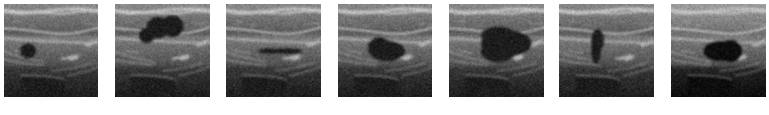

(i)

Figure 4 Output of techniques where, (a) is the original synthetic images, (b) the intentionally added speckle noise, (c) Wiener filter, (d) I. Elyasi et al., (e) G. Andria et al., (f) S.K. Randhawa et al., (g) A.K. Bedi et al., (h) SBAD, (i) Gabor, (j) DCNN, (k) proposed (continued)

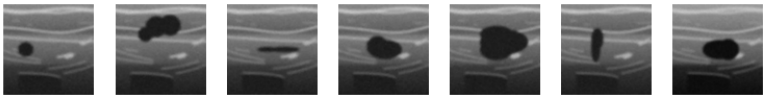

(j)

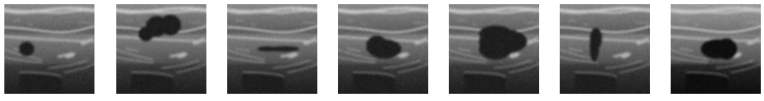

(k)

Table 3 The average S/N, M2E and SSI value of the denoised synthetic image set

Technique	$var_n = 0.1$			$var_n = 0.2$			$var_n = 0.3$		
	S/N	*M2E*	*SSI*	*S/N*	*M2E*	*SSI*	*S/N*	*M2E*	*SSI*
G. Andria (2013)	38.1	185	0.61	33.0	230	0.54	26.8	451	0.35
I. Elyasi (2016)	38.8	173	0.62	32.9	227	0.54	27.2	433	0.37
S.K. Randhawa (2019)	42.4	124	0.69	36.2	193	0.58	29.5	398	0.41
Wiener filter (2018)	44.1	116	0.73	39.6	174	0.61	33.1	266	0.53
SBAD (2021)	32.7	312	0.52	26.8	468	0.34	21.7	717	0.25
A.K. Bedi (2022)	50.7	74	0.81	43.9	168	0.73	37.7	218	0.58
Gabor (2021)	43.2	142	0.71	35.9	208	0.56	28.6	416	0.39
DCNN (2020)	53.2	60	0.83	45.7	115	0.72	35.3	289	0.55
Proposed	*52.4*	*64*	*0.83*	*47.6*	*107*	*0.78*	*42.1*	*183*	*0.70*

Since US images develop speckles during imaging, there are no clean or noise-free US images. So, we cannot apply MSE, S/N, and SSI for performance evaluation. These metrics require an image that is noise-free to quantise the recovery. But there are metrics which does not require a noise-free image for reference and are called blind or no reference image quality metrics. Blind/reference less image spatial quality evaluator (BIQE) (Mittal et al., 2012) is a blind image quality metric. It uses the basic notion that distortion destroys the spatial properties of a natural image. Another blind quality metric named natural image quality evaluator (NIQE) (Mittal et al., 2013) measures the deviation of the image from any natural image. The last metric used as a blind quality metric is the perception-based image quality evaluator (PIQE) (Venkatanath et al., 2015). It uses independent opinion-based learning to determine the quality of the image. A lower value of these metrics represents a lower distortion and means better quality.

Figure 5 Bar graph representing the S/N, SSI, and M2E for the denoising techniques proposed by G. Andria (2013), I. Elyasi (2016), S.K. Randhawa (2019), A.K. Bedi (2022), SBAD (2021), and DCNN (2020), and filters like, Wiener filter (2018) and Gabor filter (2021) (see online version for colours)

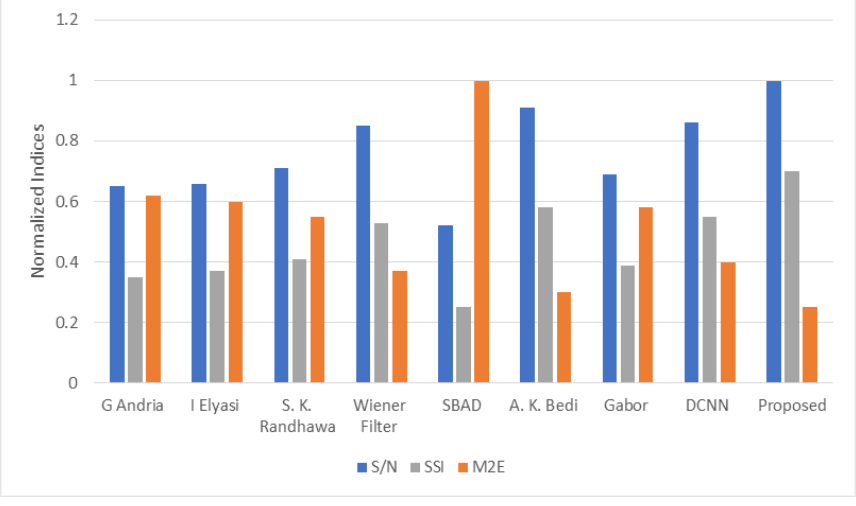

Figure 6 BIQE value of the original breast, liver, and foetus US image and corresponding denoised image (see online version for colours)

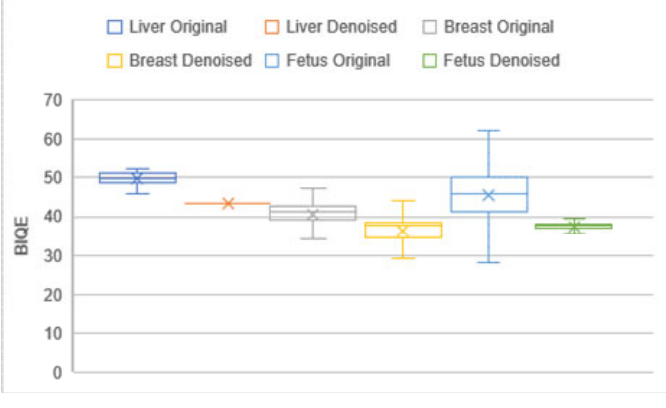

We have presented a box plot in Figures 6–8 shows the value of these metrics for the original US image and the image after denoising. Figure 6 has the box plot for the value of BIQE of US images. The first box represents the values observed across the foetus dataset. The processed foetus image's BIQE values are in the box next to the original. A similar presentation is for the liver and breast where the processed image BIQE value is right next to the original. As stated earlier, the value of all blind quality metrics is lower for a better-quality image. We can observe that the median BIQE value for original liver, foetus, and breast images are 50, 43, and 48, respectively. The median value for their corresponding processed image is 45, 38, and 38. For the processed foetus US image the median BIQE value is 20.8% lower than the original image. The highest BIQE value of

the processed image is not too from the original image. A similar presentation was adopted in Figures 7 and 8 for NIQE and PIQE, respectively. The box plot of the original image is at a higher index than the processed boxes. The median NIQE value of images is 9, 5.5, and 5.2, while the processed image is 7.2, 3, and 4.4, respectively. The denoise breast US image has a 45% improved NIQE value for the original image. For the PIQE in Figure 8, the percentage improvement in the denoised images observed was 47%, 24%, and 35%. The cross mark in each box plot represents the mean value of the box.

Figure 7 NIQE value of the original breast, liver, and foetus US image and corresponding denoised image (see online version for colours)

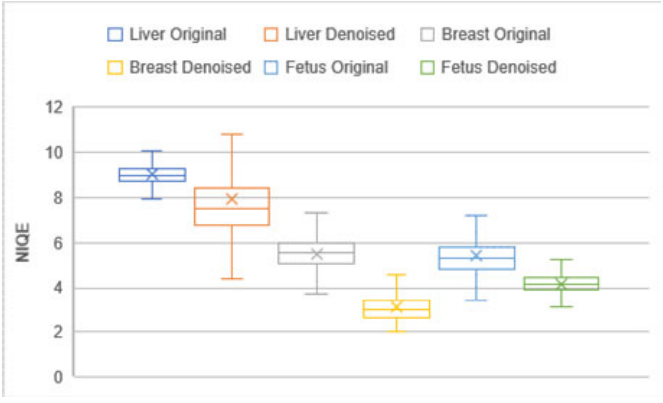

Figure 8 PIQE value of the original breast, liver, and foetus US image and corresponding denoised image (see online version for colours)

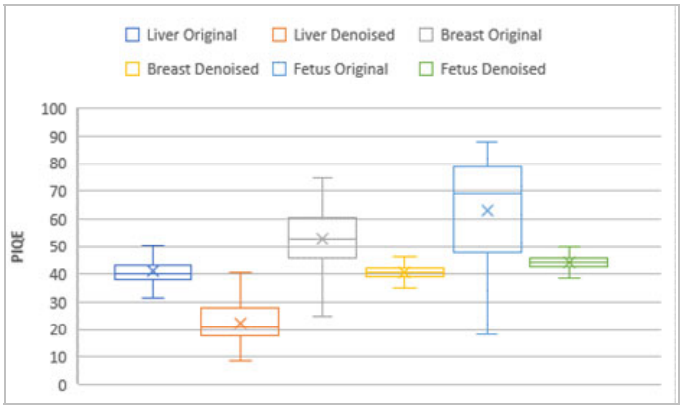

The proposed technique for denoising has a hybrid thresholding technique and a multiscale thresholding function. The hybrid threshold improves the ability to discriminate between the noisy and original pixels. And, the multiscale thresholding improves the recovery process by preserving the noise. The reference-based quality metrics has shown that the hybrid threshold and the proposed thresholding function has improved recovery compared to the standard techniques. The values of the PSNR, MSE and SSIM are lot better for the proposed technique. The values of referenceless quality metrics of the US images represents the quality of image that is being used for diagnosis.

Such quality is not acceptable for designing a computer aided detection (CAD) and might result in lousy human expert-based analysis. But after processing the US image using proposed technique the BIQE, NIQE, and PIQE has reduced substantially. These reduced values represent fewer distortion compared to the original version. With this much reduced distortions the processed image will be far more efficient as base image for CAD and human expert compared to the original image.

5 Conclusions

In this paper, we have proposed a novel speckle-noise reduction technique using wavelet thresholding. The proposed technique was tested on the medical US, standard, and synthetic images. It outperformed the best-in-class denoising techniques. For the noisy Barbara and Lena image, the proposed method had the S/N, M2E, and SSI of 34.9, 138, and 0.61, and 25.1, 529, and 0.48, respectively. And for the synthetic images the S/N, M2E, and SSI observed were 42.1, 18.3 and 0.7, respectively. The US images of the foetus, liver and breast was used in this study to analyse the outcome of the proposed technique. The blind or referenceless quality metrics like NIQE, PIQE and BIQE has shown a significant improvement in the image quality. The denoised liver US image had a 47% improved BIQE value. For the complete US image datasets, an improvement of 20.8%, 45.45%, and 47% (median) was observed in BIQE, NIQE, and PIQE, respectively.

References

Al-Dhabyani, W., Gomaa, M., Khaled, H. and Fahmy, A. (2020) 'Dataset of breast ultrasound images', *Data in Brief*, Vol. 28, p.104863, https://doi.org/https://doi.org/10.1016/j.dib.2019.104863.

Andria, G., Attivissimo, F., Lanzolla, A.M.L. and Savino, M. (2013) 'A suitable threshold for speckle reduction in ultrasound images', *IEEE Transactions on Instrumentation and Measurement*, Vol. 62, No. 8, pp.2270–2279, https://doi.org/10.1109/TIM.2013.2255978.

Anwar, S. and Rajamohan, G. (2020) 'Improved image enhancement algorithms based on the switching median filtering technique', *Arabian Journal for Science and Engineering*, Vol. 45, No. 12, pp.11103–11114, https://doi.org/10.1007/s13369-020-04983-9.

Arumugham, S., Rajagopalan, S., Rayappan, J.B.B. and Amirtharajan, R. (2019) 'Tamper-resistant secure medical image carrier: an IWT-SVD-chaos-FPGA combination', *Arabian Journal for Science and Engineering*, Vol. 44, No. 11, pp.9561–9580, https://doi.org/10.1007/s13369-019-03883-x.

Baselice, F., Ferraioli, G., Ambrosanio, M., Pascazio, V. and Schirinzi, G. (2018) 'Enhanced Wiener filter for ultrasound image restoration', *Computer Methods and Programs in Biomedicine*, Vol. 153, pp.71–81, https://doi.org/https://doi.org/10.1016/j.cmpb.2017.10.006.

Bedi, A.K. and Sunkaria, R.K. (2022) 'Ultrasound speckle reduction using adaptive wavelet thresholding', *Multidimensional Systems and Signal Processing*, Vol. 33, No. 2, pp.275–300, https://doi.org/10.1007/s11045-021-00799-4.

Bini, A.A. (2021) 'Speckle reducing non-local variational framework based on maximum mean discrepancy', *Arabian Journal for Science and Engineering*, Vol. 46, No. 9, pp.8273–8285, https://doi.org/10.1007/s13369-021-05355-7.

Bini, A.A. and Bhat, M.S. (2014) 'Despeckling low SNR, low contrast ultrasound images via anisotropic level set diffusion', *Multidimensional Systems and Signal Processing*, Vol. 25, No. 1, pp.41–65, https://doi.org/10.1007/s11045-012-0184-5.

Burgos-Artizzu, X.P., Coronado-Gutiérrez, D., Valenzuela-Alcaraz, B., Bonet-Carne, E., Eixarch, E., Crispi, F. and Gratacós, E. (2020) 'Evaluation of deep convolutional neural networks for automatic classification of common maternal fetal ultrasound planes', *Scientific Reports*, Vol. 10, No. 1, p.10200, https://doi.org/10.1038/s41598-020-67076-5.

Chang, S.G., Yu, B. and Vetterli, M. (2000) 'Adaptive wavelet thresholding for image denoising and compression', *IEEE Transactions on Image Processing*, Vol. 9, No. 9, pp.1532–1546, https://doi.org/10.1109/83.862633.

Chen, H., Xu, H., Shi, P., Gong, Y., Qiu, Z., Shi, L. and Zhang, Q. (2021) '3-D Gabor-based anisotropic diffusion for speckle noise suppression in dynamic ultrasound images', *Physical and Engineering Sciences in Medicine*, Vol. 44, No. 1, pp.207–219, https://doi.org/10.1007/s13246-020-00969-x.

Chen, Y. and He, T. (2021) 'Image denoising via an adaptive weighted anisotropic diffusion', *Multidimensional Systems and Signal Processing*, Vol. 32, No. 2, pp.651–669, https://doi.org/10.1007/s11045-020-00760-x.

Donoho, D.L. (1995) 'De-noising by soft-thresholding', *IEEE Transactions on Information Theory*, Vol. 41, No. 3, pp.613–627, https://doi.org/10.1109/18.382009.

Elyasi, I., Pourmina, M.A. and Moin, M-S. (2016) 'Speckle reduction in breast cancer ultrasound images by using homogeneity modified bayes shrink', *Measurement*, Vol. 91, pp.55–65, https://doi.org/https://doi.org/10.1016/j.measurement.2016.05.025.

Jing-Yi, L., Hong, L., Dong, Y. and Yan-Sheng, Z. (2016) 'A new wavelet threshold function and denoising application', *Mathematical Problems in Engineering*, p.3195492, https://doi.org/10.1155/2016/3195492.

Khatkar, K. and Kumar, D. (2015) 'Biomedical image enhancement using wavelets', *Procedia Computer Science*, Vol. 48, pp.513–517.

Kokil, P. and Sudharson, S. (2020) 'Despeckling of clinical ultrasound images using deep residual learning', *Computer Methods and Programs in Biomedicine*, Vol. 194, p.105477, https://doi.org/https://doi.org/10.1016/j.cmpb.2020.105477.

Luo, L., Zhao, Z., Li, X. and Feng, X. (2019) 'A stochastic image denoising method based on adaptive patch-size', *Multidimensional Systems and Signal Processing*, Vol. 30, No. 2, pp.705–725, https://doi.org/10.1007/s11045-018-0577-1.

Mittal, A., Moorthy, A.K. and Bovik, A.C. (2012) 'No-reference image quality assessment in the spatial domain', *IEEE Transactions on Image Processing*, Vol. 21, No. 12, pp.4695–4708, https://doi.org/10.1109/TIP.2012.2214050.

Mittal, A., Soundararajan, R. and Bovik, A.C. (2013) 'Making a 'completely blind' image quality analyzer', *IEEE Signal Processing Letters*, Vol. 20, No. 3, pp.209–212, https://doi.org/10.1109/LSP.2012.2227726.

Nabil, T. (2013) 'Iterative projective Gabor method for images filtering', *Arabian Journal for Science and Engineering*, Vol. 38, No. 10, pp.2745–2753, https://doi.org/10.1007/s13369-012-0489-6.

Nair, R.R. and Singh, T. (2022) 'Optimal wavelet-based multi-modal medical image fusion with quantitative analysis for colour images using different colour models', *International Journal of Biomedical Engineering and Technology*, Vol. 40, No. 3, pp.262–288, https://doi.org/10.1504/IJBET.2022.10051150.

Perumal, N. and Thiruvenkadam, K. (2022) 'Brain tumour segmentation from magnetic resonance images using improved FCM and active contour model', *International Journal of Biomedical Engineering and Technology*, Vol. 39, No. 2, p.188, https://doi.org/10.1504/IJBET.2022.10048624.

Priestly Shan, B., Jeba Shiney, O. and Singh, J.A.P. (2021) 'An improved speckle noise reduction scheme using switching and flagging of noisy data for pre-processing of ultrasonograms in detection of down syndrome during first and second trimesters', *International Journal of Biomedical Engineering and Technology*, Vol. 37, No. 2, p.105, https://doi.org/10.1504/IJBET.2021.10043165.

Randhawa, S.K., Sunkaria, R.K. and Puthooran, E. (2019) 'Despeckling of ultrasound images using novel adaptive wavelet thresholding function', *Multidimensional Systems and Signal Processing*, Vol. 30, No. 3, pp.1545–1561, https://doi.org/10.1007/s11045-018-0616-y.

Singh, M.K., Saini, I., Sood, N. and Saini, J. (2021) 'A sub-band anisotropic diffusion technique for de-speckling of ultrasound images of breast cancer', *AIJR Proceedings*, pp.72–77.

Talbar, S.N., Handique, A., Dutande, P.V., Baid, U., Paul, S. and Mourya, G.K. (2022) 'Modified U-Net for fully automatic liver segmentation from abdominal CT-image', *International Journal of Biomedical Engineering and Technology*, Vol. 40, No. 1, p.1, https://doi.org/10.1504/IJBET.2022.10050023.

Ultrasound Data of a Variety of Liver Masses (B-mode-and-CEUS-Liver) – The Cancer Imaging Archive (TCIA) Public Access – Cancer Imaging Archive Wiki (n.d.) [online] https://wiki.cancerimagingarchive.net/pages/viewpage.action?pageId=61080617#61080617171ba531fc374829b21d3647e95f532c (accessed 19 July 2022).

Venkatanath, N., Praneeth, D., Chandrasekhar, M.B., Channappayya, S.S. and Medasani, S.S. (2015) 'Blind image quality evaluation using perception based features', *2015 Twenty First National Conference on Communications (NCC)*, pp.1–6, https://doi.org/10.1109/NCC.2015.7084843.

Venkatesan, B. and Ragupathy, U.S. (2022) 'Integrated fusion framework using hybrid domain and deep neural network for multimodal medical images', *Multidimensional Systems and Signal Processing*, Vol. 33, No. 3, pp.819–834, https://doi.org/10.1007/s11045-021-00813-9.

Vidakovic, B. (1998) 'Nonlinear wavelet shrinkage with Bayes rules and Bayes factors', *Journal of the American Statistical Association*, Vol. 93, No. 441, pp.173–179, https://doi.org/10.1080/01621459.1998.10474099.

Wilcox, R.R. (2022) 'Chapter 3 – estimating measures of location and scale', in Wilcox, R.R. (Ed.): *Introduction to Robust Estimation and Hypothesis Testing*, 5th ed., pp.45–106, Academic Press, Massachusetts, https://doi.org/https://doi.org/10.1016/B978-0-12-820098-8.00009-9.

Yadav, D.M. and Ganvir, N.N. (2022) 'An automatic detection of microcalcification in mammogram images using neuro-fuzzy classifier', *International Journal of Biomedical Engineering and Technology*, Vol. 40, No. 2, p.130, https://doi.org/10.1504/IJBET.2022.10050143.

Yu, C., Zhang, C. and Xie, L. (2012) 'A multiplicative Nakagami speckle reduction algorithm for ultrasound images', *Multidimensional Systems and Signal Processing*, Vol. 23, No. 4, pp.499–513, https://doi.org/10.1007/s11045-012-0173-8.